ADVANCES IN ATMOSPHERIC SCIENCES, VOL. 29, NO. 6, 2012, 1318–1329

Comparison of Precipitation Observations from a Prototype Space-based Cloud Radar and Ground-based Radars

LIU Liping*[1] (刘黎平), ZHANG Zhiqiang[1] (张志强), YU Danru[2] (于丹茹), YANG Hu[3] (杨 虎), ZHAO Chonghui[2] (赵崇辉), and ZHONG Lingzhi[1] (仲凌志)

[1]*State Key Laboratory of Severe Weather, Chinese Academy of Meteorological Sciences, Beijing* 100081

[2]*Science and Technology on Milimeter-wave Laboratory, Beijing* 100854

[3]*National Satellite Meteorological Center, Beijing* 100081

(Received 11 November 2011; revised 13 March 2012)

ABSTRACT

A prototype space-based cloud radar has been developed and was installed on an airplane to observe a precipitation system over Tianjin, China in July 2010. Ground-based S-band and Ka-band radars were used to examine the observational capability of the prototype. A cross-comparison algorithm between different wavelengths, spatial resolutions and platform radars is presented. The reflectivity biases, correlation coefficients and standard deviations between the radars are analyzed. The equivalent reflectivity bias between the S- and Ka-band radars were simulated with a given raindrop size distribution. The results indicated that reflectivity bias between the S- and Ka-band radars due to scattering properties was less than 5 dB, and for weak precipitation the bias was negligible. The prototype space-based cloud radar was able to measure a reasonable vertical profile of reflectivity, but the reflectivity below an altitude of 1.5 km above ground level was obscured by ground clutter. The measured reflectivity by the prototype space-based cloud radar was approximately 10.9 dB stronger than that by the S-band Doppler radar (SA radar), and 13.7 dB stronger than that by the ground-based cloud radar. The reflectivity measured by the SA radar was 0.4 dB stronger than that by the ground-based cloud radar. This study could provide a method for the quantitative examination of the observation ability for space-based radars.

Key words: space-based cloud radar, observational capability, field experiment, cloud observation

Citation: Liu, L. P., Z. Q. Zhang, D. R. Yu, H. Yang, C. H. Zhao, and L. Z. Zhong, 2012: Comparison of precipitation observations from a prototype space-based cloud radar and ground-based radars. *Adv. Atmos. Sci.*, **29**(6), 1318–1329, doi: 10.1007/s00376-012-1233-6.

1. Introduction

Ground-based radar, airborne radar and space-based radar are very important for detecting the 3-D structure of cloud systems. Short wavelength radar, compared to longer wavelength radar, possesses better sensitivity for the detection of small hydrometeors because the backscattering cross section of cloud droplets is proportional to λ^{-4} for Rayleigh scattering. Weather radars (X-, C- and S-band) are designed to detect precipitation systems, while Ka-band cloud radar is especially well suited for sensitive and accurate measurements of nonprecipitating and weak precipitating cloud features at fine spatial and temporal resolutions. W-band cloud radar is suitable for weak clouds, such as cumulus and cirrus.

Research on millimeter-wavelength radars started in the 1950s (Atlas, 1954). Not long after that, vertical point cloud radar at a wavelength of 1.25 cm was developed by the USAF (United States Air Force) in the 1960s and used to observe the frequencies of various cloud types and their typical echo characteristics, but was unable to detect radial velocity (Plank et al., 1955; Paulsen et al., 1970). Until

*Corresponding author: LIU Liping, lpliu@cams.cma.gov.cn

the 1980s, more advancements came when the scanable Ka-band cloud radar system was developed by the NOAA（National Oceanic and Atmospheric Administration）Environmental Technology Laboratory. Advanced antenna and polarization technologies were used in this radar system to enhance its detection ability. Further technological advances then allowed the development of shorter wavelength cloud radar, and a W-band cloud radar was also built for weak cloud detection (Lhermitte, 1987; Kropfli et al., 1990; Kropfli and Kelly, 1996).

In 1990, the University of Wyoming developed ground-based W-band cloud radar system and used in experiment campaigns (Pazmany et al., 1994a, 1994b; Vail et al., 1995). The dual wavelength (33 GHz and 95 GHz) cloud radar (CPRS) from UMass was also used to detect the phenomenon of undercooling raindrops (Sekelsky and McIntosh, 1996). Indeed, this technique is useful for observing both ice clouds and super-cold water droplets. In 1996, a 35-GHz millimeter-wave cloud radar (MMCR) system was designed to provide detailed, long-term observations of nonprecipitating and weak precipitating clouds at the Cloud and Radiation Test (CART) bed site of the US Department of Energy's Atmospheric Radiation Measurement (ARM) Program (Moran et al., 1998; Kollias et al., 2007).

Space-based active remote sensing equipment, such as the TRMM's PR (Tropical Rainfall Measuring Mission satellite，Precipitation Radar), which operates at a wavelength of 2.17 cm, and the W-band cloud radar on board Cloudsat, have also been used to detect the 3-D structures of clouds and precipitation at the global scale. The 3-D detection capability of passive remote sensing systems for measuring precipitation has improved greatly, and the observation area of radar has expanded (Graeme et al., 2002; Marchand et al., 2008). Bolen and Chandrasekar (2000) developed a reflectivity comparison algorithm between space-based and ground-based radar to evaluate, qualitatively, the ability of space-based radar observations. Similarly, the space-based W-band cloud radar has also been studied (Danne et al., 1999; Hamazu et al., 2003; O'Connor et al., 2004).

In China, a new generation weather radar network operating at the C and S bands (CINRAD) started to be built in 1998 and has been used to observe and provide warnings for imminent severe weather events. Meanwhile, Ka-band cloud radars have also been used to observe cloud features. A Ka-band ground-based cloud radar with Doppler and polarization functions was independently developed by the State Key Laboratory of Severe Weather, Chinese Academy of Meteorological Sciences, in collaboration with the No. 23 Institute of the Second Academy of China Aerospace Science and Industry Corporation. The system has been used to observe clouds and precipitation in a field experiment, and the data were used to study microphysical parameters (Zhong et al., 2011). The Wuhan Institute of Heavy Rainfall, the China Meteorological Administration and the Nanjing University of Information Science and Technology, collectively developed two Ka-band cloud radars. Meanwhile, a project to develop a space-based cloud/rain radar was already underway as part of the Meteorological Satellite Program, with a prototype having been developed and flown in an airplane to observe a precipitation system over Tianjin in July 2010.

In this paper, the ground-based cloud radar at the State Key Laboratory of Severe Weather, Chinese Academy of Meteorological Sciences and the S-band operational Doppler radar in Tianjin were used to examine the reflectivity bias, and its vertical profile, in the prototype space-based cloud radar. A cross comparison of reflectivity at different resolutions, scan strategies and wavelengths is reported, and the difference between observed reflectivity in the S- and Ka-band radars, due to scattering properties, is analyzed.

2. Data processing and analysis scheme

The prototype space-based cloud radar was developed for the Ka band (35.5 GHz) and was installed on an airplane (referred to as airborne cloud radar) to observe the clouds and precipitation below the airplane. The beam width, scan range and gate spacing of the radar were 0.9°, ±18° and 48 m, respectively. A pulse compression and pulse width of 20 μs was chosen for the observation of the 3-D structure of the clouds and precipitation.

The Ka-band ground-based cloud radar, whose parameters are listed in Table 1, was located at 38.85°N, 117.63°E. The vertical point mode was used during the observation period for comparison of the vertical profile of reflectivity with the airborne cloud radar. In addition, data from the S-band operational Doppler radar (SA) in Tianjin (39.044°N, 117.717°E, altitude of 70.3 m) were also applied to an analysis of the reflectivity bias and spatial variability along the airplane route and at the location of the ground-based cloud radar.

The operational S-band radar was calibrated by the radar company. For the operational observation, the calibration was conducted at each volume scan beginning with the inner calibration system. The ground-based cloud radar had previously been calibrated when being used for other scientific experiments. It worked at pulse widths of 20 μs, FFT points of 256 and a pulse

Table 1. Characteristics of the Ka-band (35 GHz) cloud radar.

Antenna		Receiver	
Diameter	1.3m	Mode	Transmit H, receive H and V
Gain	50 dB	Sensitivity	$\leqslant -98.4$ dBm
Beam width	0.44°	Noise figure	$\leqslant 5.6$ dB
First side lobe	< -30 dB	Dynamic range	70.0 dB
Cross polarization isolation	> 33 dB		
Transmitter		Data processing system	
Frequency	Ka band	Range gate number	500
Peak power	600 W	Range resolution	30 m or 60 m
Pulse length	0.3, 1.5, 20, 40 μs	Base parameters	Z, $V_{\rm r}$, $S_{\rm W}$, $L_{\rm DR}$
Pulse repetition frequency	2500 or 5000 Hz	Processing method	FFT, PPP
Polarization	Horizontal	FFT points	128, 256, 512
		Pulse compression performance	side lobe<30 dB

Note: Z: reflectivity factor; $V_{\rm r}$: radial velocity; $S_{\rm w}$: spectral width; $L_{\rm DR}$: linear depolarization radito.

compression ratio of 200 in the field experiment. The cloud radar data were also compared with the data from an SA radar in Guangdong in 2008 (Zhong et al., 2011). In a similar way to the calibration of the ground-based cloud radar, the airborne cloud radar was also tested. Absolute calibration of reflectivity was conducted with a ground-based Active Cavity Radiometer (ACR).

The field experiment was carried out on 10 July 2010 by the National Meteorological Satellite Center, Chinese Academy of Meteorological Sciences, and the No. 25 Institute of the Second Academy of China Aerospace Science and Industry Corporation. The airborne cloud radar, ground-based SA radar and cloud radar were used to observe the weak precipitation systems. The airplane flew from east to west and its observation routes are shown in Table 2.

To avoid interference between the ground-based radar and airborne cloud radar, and destroying the cloud radar system, the ground-based cloud radar was located away from the airplane routes by a certain distance. Minimum distances between the ground-based cloud radar and the three airplane routes were 2 km, 9 km and 3 km, respectively. The distance between the SA radar and the ground-based cloud radar was 23 km. The minimum distance between the SA radar and the three airplane routes was 33 km.

For quantitative comparisons, differences between the observation mode and the wavelength among the three radars should be considered. The SA radar performed volume scans, with nine elevation angles, once every 6 min. The SA radar raw data were interpolated onto a Cartesian grid with a 0.01° interval in the horizontal direction and 0.5 km in the vertical direction. The reflectivity profiles over the ground-based cloud radar and the cross section along the airplane route were retrieved from the grid radar data of the SA radar. The SA radar data matched with those of the ground-based cloud and airborne cloud radars very well in time and space; however, its horizontal and vertical spatial resolutions were larger than those of both cloud radars. The airborne cloud and ground-based cloud radars were able to resolve similar spatial and temporal resolution data, but the observation directions were opposite to each other, which could have introduced different propagation attenuations. In addition, the observation locations of the airborne cloud radar and ground-based cloud radar were different so that the spatial variation of precipitation would introduce a comparison bias between the airborne cloud radar and the ground-based cloud radar. Another important factor is the bias introduced by the different wavelengths. Large drizzle particles could produce the differences in observed reflectivity between the S-band and Ka-band radars.

The main steps involved in the data processing and analysis used in this study were:

(1) Airborne radar data processing

Table 2. Airborne radar observation routes.

Approx. time of flight (LST)	Latitude	Longitude range	Route number
0918–0921	38.87°N	117.42°–117.79°E	I(A–B)
0933–0936	38.76°N	117.58°–117.79°E	II(C–D)
0940–0936	38.87°N	117.41°–117.76°E	III(A–B)
1021–1024	38.82°N	117.55°–117.75°E	IV(E–F)

The airborne radar performed cross-track scanning toward the ground with an intersecting angle of ±18° once every 0.5 s. The scanning section was normal to the airplane's movement. To balance the spatial differences of observation data between the SA and airborne radars, and to simplify the comparison, the reflectivity in the cross section with ±18° scanning was averaged across the track to obtain the reflectivity vertical profiler. These profiles were calculated based on the aircraft's altitude and radar scan status during data processing.

The altitude (height) of any pixel of airborne cloud radar data can be expressed by

$$H_0 \times \cos(\alpha + \beta) \times \cos(\gamma) \,, \tag{1}$$

where α, β, γ and H_0 are the scan angle of the antenna, the roll angle, elevation angle and the flight height of the aircraft, respectively. R is distance between observe target and airborne radar.

(2) SA radar data processing

The SA radar data remap proposed by the State Key Laboratory of Severe Weather at the Chinese Academy of Meteorological Sciences (Wang et al., 2009) was used to interpolate the SA radar raw data onto a Cartesian grid with a horizontal and vertical resolution of 0.01° and 0.5 km, respectively. Using the processed reflectivity grid data, we were able resolve the vertical cross section of reflectivity along the airplane's route and the vertical profiler at the location of the ground-based cloud radar. The cross section and vertical profiler would then be used to compare with the airborne and ground-based cloud radars.

(3) Ground-based cloud radar data processing

The time-averaged reflectivity for the ground-based cloud radar for once every 6 min was compared with the reflectivity profile of the SA radar data over the ground-based cloud radar.

(4) Comparison between airborne cloud radar and SA radars

The airborne cloud radar observed 530 profilers at a vertical resolution of 0.1 km along each observation route. In this region, the SA radar observed 21–38 reflectivity profilers (0.01°, 0.5 km) according to the route extension. The two kinds of profilers were averaged along each route to examine the ability of the airborne cloud radar to examine vertical structure. The reflectivity profilers from the airborne cloud radar were interpolated onto the SA grid. The data on the same pixels were used to analyze the bias, correlation and variations between both radars.

(5) Comparison between the ground-based cloud and SA radars

The averaged vertical profiler of reflectivity recorded by the ground-based cloud radar once every 6 min was compared with the vertical profiler of SA reflectivity over the ground-based cloud radar. The time-averaged reflectivity for the ground-based cloud radar was interpolated onto the SA radar grid and compared with the reflectivity recorded by the SA radar.

(6) Comparison between the ground-based cloud radar and the airborne cloud radars

The averaged vertical profiler of reflectivity recorded by the airborne cloud radar closest to the ground-based cloud radar (4 km in horizontal distance) was chosen to compare with the profilers from the ground-based radar data for the same time. The reflectivity bias due to the spatial difference was analyzed with the SA radar data at two locations.

3. Simulation of reflectivity for S and Ka bands

The contribution of wavelength to the reflectivity bias should be discussed. The scattering properties of large hydrometeor particles for the Ka-band wavelength do not obey Rayleigh scattering, which would produce an observation bias of reflectivity between the S-band and Ka-band radars. The Extended Boundary Condition Method (Barber and Yeh, 1975) was used to calculate the back scattering cross sections of drizzle drops for S- and Ka-band radar waves. The reflectivity bias of cloud and weak precipitation for S and Ka bands were simulated under the assumption of gamma drop size distribution proposed by Ulbrich (1983), Chandrasekar et al. (1990) and Scarchilli et al. (1993). The gamma distribution assumption can be expressed by

$$N(D) = N_0 D^m \exp\left[\frac{-(3.67+m)\times D}{D_0}\right] \,, \tag{2}$$

where D is diameter of raindrop. The variational span of N_0 (m^{-3} mm^{-1-m}), m and D_0 (mm) can be expressed by

$$-1 < m < 4 \,; \tag{3}$$

$$10^{3.2-m}\exp(2.8m) < N_0 < 10^{4.6-m}\exp(3.57m) \tag{4}$$

$$0.5 < D_0 < 2.5 \,. \tag{5}$$

The drop size distribution and parameter variations defined by Eqs. (2)–(5) can be used to simulate the actual cloud and weak precipitation processes.

Figure 1 shows the backscattering cross section of liquid particles for the S and Ka bands and their ratio. It can be observed that the back scattering sections for the Ka band are larger than those of the S band. Although the sections for the Ka band increase with in-

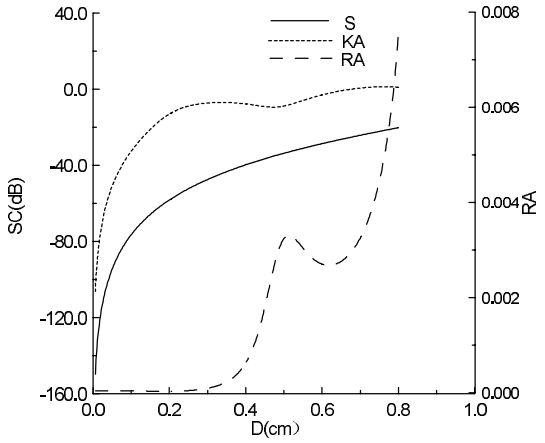

Fig. 1. Scattering cross sections of liquid spherical hydrometeors for the S-band (solid line), Ka-band (short dashed line) and their ratio (long dashed line). The units of the scattering cross sections are cm^2 and are expressed in dB on the y axis.

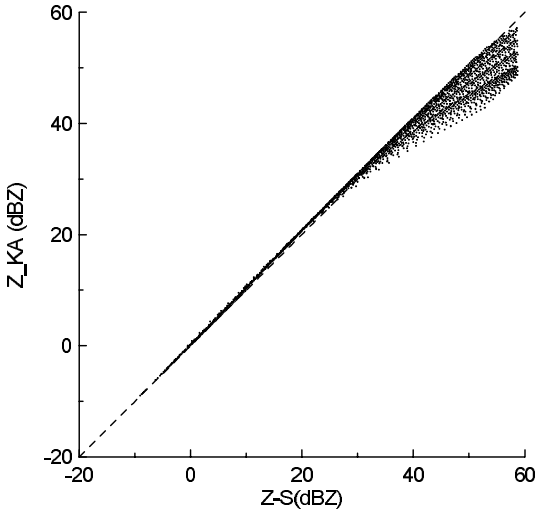

Fig. 2. Simulated reflectivity for the S-band (x axis) and Ka-band radar (y axis).

creasing drop size, the ratio decreases when liquid particle diameters are greater than 0.3 cm. The difference between the scattering properties for the S and Ka bands means that the contributions of large drops to equivalent reflectivity for Ka are less than that for the S band, which could reduce the measured reflectivity for the Ka band. The relationships of equivalent reflectivity for both bands are shown in Fig. 2, which shows that the differences of equivalent reflectivity between both bands are few when the reflectivity is less than 30 dBZ. However, the equivalent reflectivity for the S band becomes stronger than that for the Ka band when the reflectivity is beyond this range; for example, the 40 dBZ for the S band corresponds with 35 dBZ for the Ka band. The above results are a theoretical base for discussion of reflectivity bias due to the different wavelength.

4. Comparative analysis of observational reflectivity for airborne cloud radar, ground-based cloud radar and ground-based S-band radar

Figure 3 shows the CAPPI (Constant Altitude Plan Position Indicator) for reflectivity at 3 km above mean sea level (MSL) at 0918 LST and 1021 LST 10

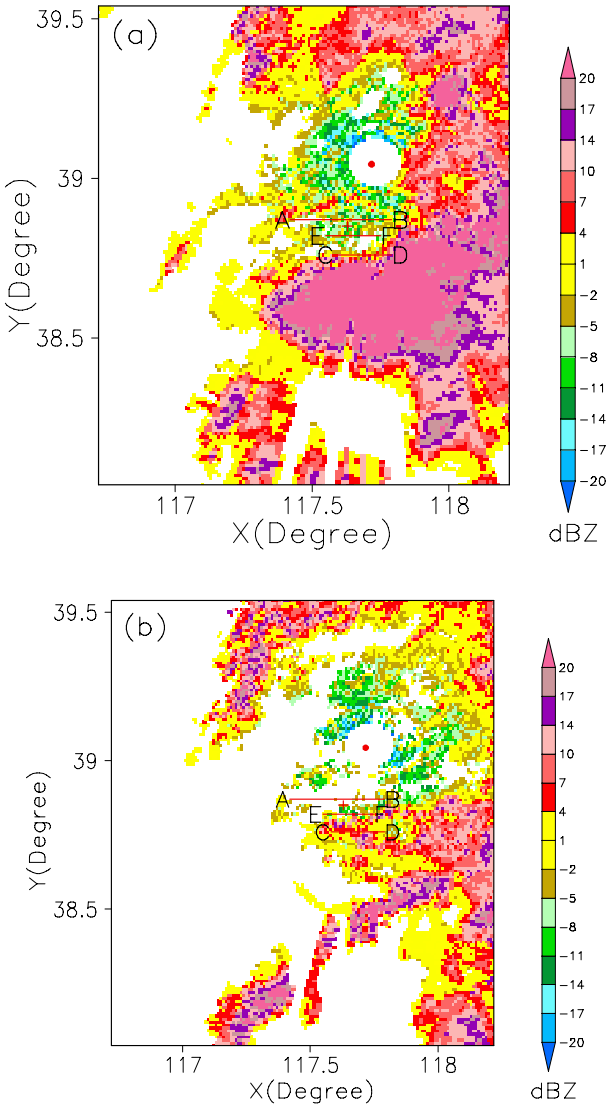

Fig. 3. CAPPI for reflectivity at 3 km MSL at 0918 LST (a) and 1021 LST (b) The observation route of the airplane is the red line; "+" depicts the location of the ground-based cloud radar; and the SA radar is marked by "•".

July 2010. The locations of the S-band radar and ground-based cloud radar, as well as the four airplane routes, are also marked on the figure. Routes I and III in Table 2, marked by AB in Fig. 3, have the same latitude. We can see that the stratiform cloud system moved to the east and had a maximum reflectivity of 35 dBZ, and the height echo top extended up to approximately 6 km MSL. The observed precipitation was weak and located at the northern edge of a precipitation system. Although the reflectivity biases due to different wavelengths could be neglected, large temporal and spatial variation of reflectivity would still cause some difference for quantitative analysis, especially the error induced by different observation geometries. Therefore, we use the SA radar data as a "bridge" to detect the spatial variation of reflectivity.

4.1 *Comparison of reflectivity and its vertical profile between the airborne cloud radar and SA radar*

The vertical cross section of reflectivity observed with the airborne cloud radar and the SA radar along the airplane route at 0918 LST is illustrated in Fig. 4. The SA radar observed a minimum reflectivity of approximately −15 dBZ and an echo top of 6 km MSL, while the minimum reflectivity observed with the airborne radar was approximately −18 dBZ and the bright band was relatively obvious at 4 km MSL. Both radars were able to catch a similar pattern of reflectivity, e.g. two strong echoes centers located at 117.70°E and 117.76°E. It can be observed from the vertical structure that reflectivity with the airborne radar had significant increases with decreasing height. It is notable that the increase of reflectivity below 1.5 km MSL was due to the contribution of ground clutter from the antenna side lobe.

To examine the vertical structure by both radars, the mean vertical profilers of reflectivity along the four routes (defined in Table 1) observed by the airborne cloud radar and SA radar are shown in Fig. 5. Each profiler observed by the airborne cloud radar was calculated from 340 profilers. For the SA radar, the four mean profilers are averaged from 38, 22, 36 and 21 vertical profilers, respectively. The patterns of reflectivity variation caught by both radars are similar between 1.5 and 5 km MSL, but the airborne cloud radar was able to observe stronger reflectivity and more detailed structures, and the SA radar smoothed the profiler in

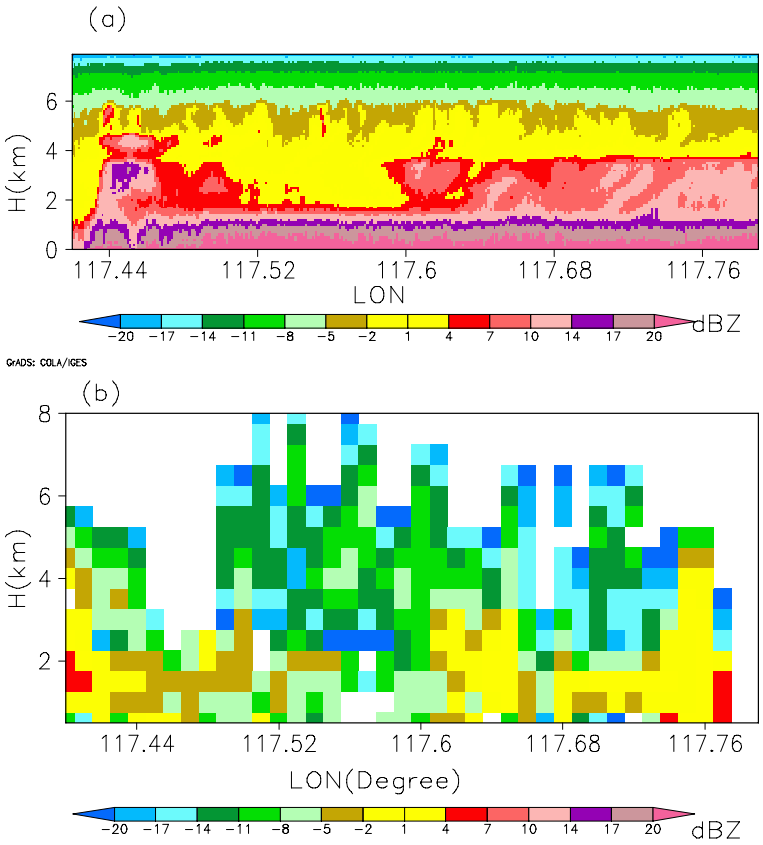

Fig. 4. Cross sections of reflectivity with the airborne cloud radar (CS1) (a) and the SA radar (CS2) (b) along the airplane's route.

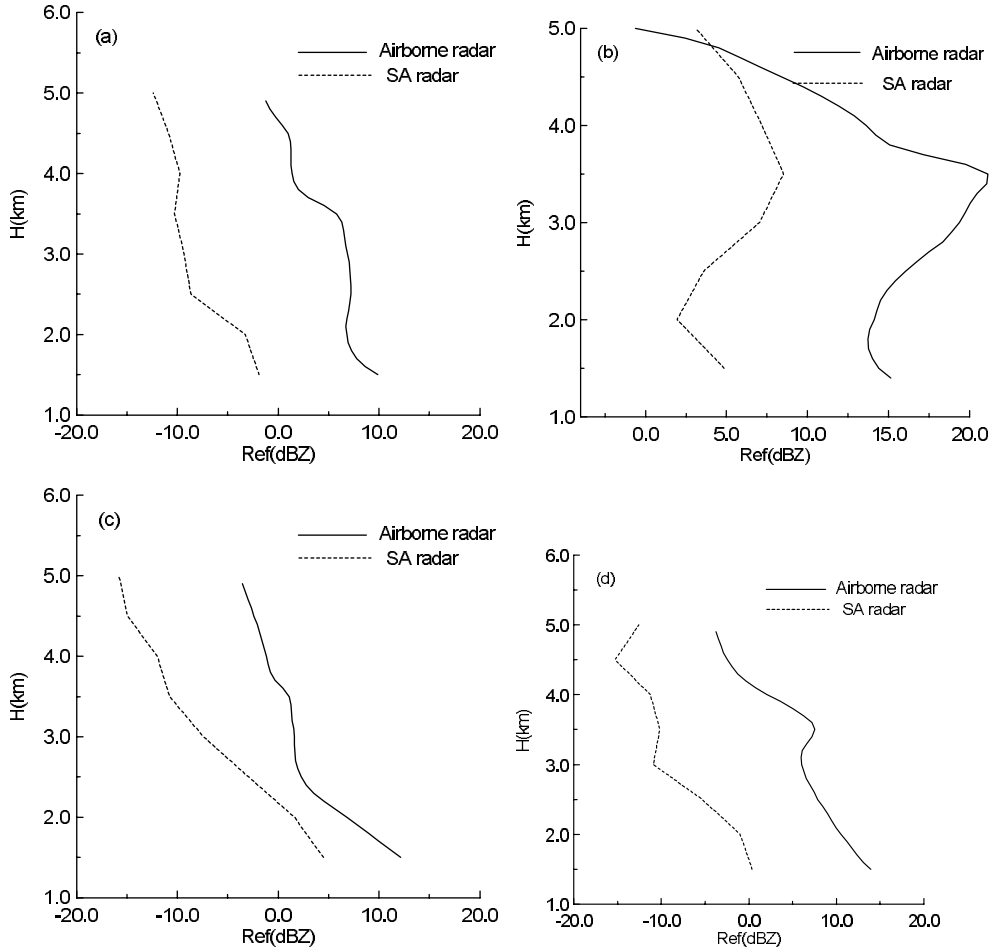

Fig. 5. The averaged vertical profilers of reflectivity with the airborne cloud radar and SA radar along Route IV and at time intervals (a) 0918 LST, Route I; (b) 0933 LST, Route II; (c) 0940 LST, Route III; and (d) 1021 LST, Route IV. The solid and dashed lines represent the airborne and SA radars, respectively.

the sharp variations of reflectivity due to the beam width.

For quantitative comparison, the reflectivity measured by airborne cloud radar for four routes was interpolated to the SA grid (0.01°, 0.5 km). The scattergram for 597 pairs of reflectivity by both radars are shown in Fig. 6. The statistical parameters were calculated with these grid data. The airborne cloud radar was able to observe stronger reflectivity than the SA radar, with the averaged bias of reflectivity for the four routes between the two radars being 10.9 dB (correlation coefficient of 0.57 and standard deviation of 6.5 dBZ). Table 3 lists these parameters for each route. In the statistical analysis, only those pixels where both radars had observation data were considered. The probability distributions for reflectivity by both of radars are shown in Fig. 7, from which we can conclude that the SA radar observed more samples in strong reflectivity regions, and the airborne cloud

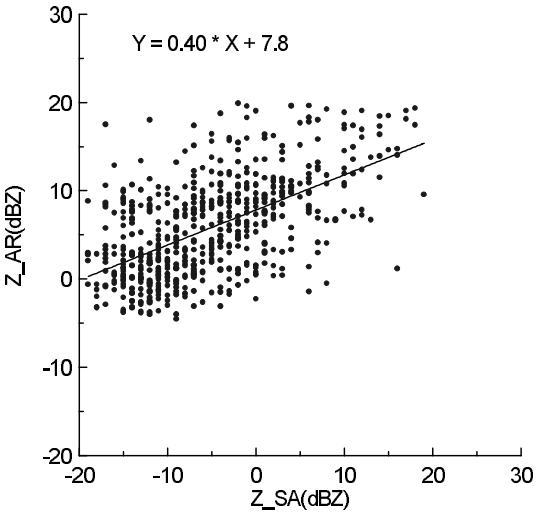

Fig. 6. Scattergram for 597 pairs of reflectivity recorded by the SA radar and airborne cloud radar (AR).

Table 3. The bias, correlation coefficient and standard deviation for reflectivity by the airborne and SA radars at altitudes between 1.5 and 5 km MSL.

Route number	Samples	Bias (Z1–Z2)	Correlation coefficient	Standard deviation
I	251	12.7	0.40	5.7
II	103	7.4	0.46	7.6
III	155	9.4	0.67	6.5
IV	88	13.1	0.57	5.9
Summation	597	10.9	0.57	6.5

Note: Z1—averaged reflectivity recorded by the airborne cloud radar; Z2—averaged reflectivity recorded by the SA radar.

Table 4. The bias, correlation coefficient and standard deviation for reflectivity recorded by the ground-based cloud radar and the SA radar at altitudes between 1.0 and 5 km MSL.

Time (LST)	Samples	Bias (Z3–Z2)	Correlation coefficient	Standard deviation
0907	11	−1.8	0.96	1.39
0914	11	1.1	0.92	1.73
Total	22	−0.4	0.91	2.1

Note: Z3—averaged reflectivity recorded by the ground-based cloud radar.

radar observed more samples in weak reflectivity regions.

4.2 *Comparison of reflectivity and its vertical profile between the ground-based cloud radar and SA radar*

The reflectivity with the ground-based cloud radar was time-averaged for 6 min and then interpolated onto the SA vertical grid. The vertical profilers of reflectivity observed with the ground-based cloud radar and SA radar over the cloud radar at 0907 LST and 0914 LST are given in Fig. 8. The scattergram for both kinds of reflectivity is also shown. After 0920 LST, the reflectivity became too weak and shallow for the SA radar. Table 4 lists the bias, correlation coefficient and standard deviation between the ground-based cloud radar and the SA radar at altitudes between 1.0 and 5.0 km MSL. It can be seen that the variation of reflectivity with altitude observed by the ground-based cloud radar is relatively consistent with the SA radar. The averaged bias of reflectivity is about −0.4 dB. The correlation is good for these cases.

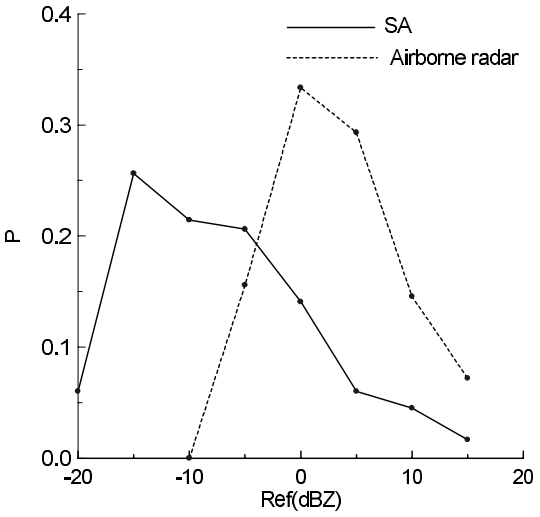

Fig. 7. Probability distributions for reflectivity of the SA radar and airborne cloud radar (AR).

4.3 *Comparison of reflectivity and its vertical profile between the ground-based cloud radar and airborne cloud radar*

The flight data closest to the ground-based radar were chosen for comparison purposes. In addition, the variation of reflectivity in the airplane and ground-based radar positions were analyzed using the SA radar. The ground-based cloud radar data at 0914 LST to 0921 LST and 1015 LST to 1022 LST were averaged to obtain two reflectivity profiles. The reflectivity profiles by the airborne cloud radar were corrected to the position of the ground-based radar by subtracting the reflectivity differences between the two positions. Similar to the ground-based cloud radar data, the airborne cloud radar data at 0918 LST to 0921 LST and 1021 LST to 1024 LST were averaged to obtain two reflectivity profiles. In these two periods, the distance between the airborne and ground-based cloud radars was less than 4 km in horizontal direction. Figures 9a and b provide a comparison of corrected reflectivity between the ground-based and airborne radars for the two periods. Considering that the location of the aircraft radar and ground-based radar was different, the averaged reflectivity profiles along the airplane

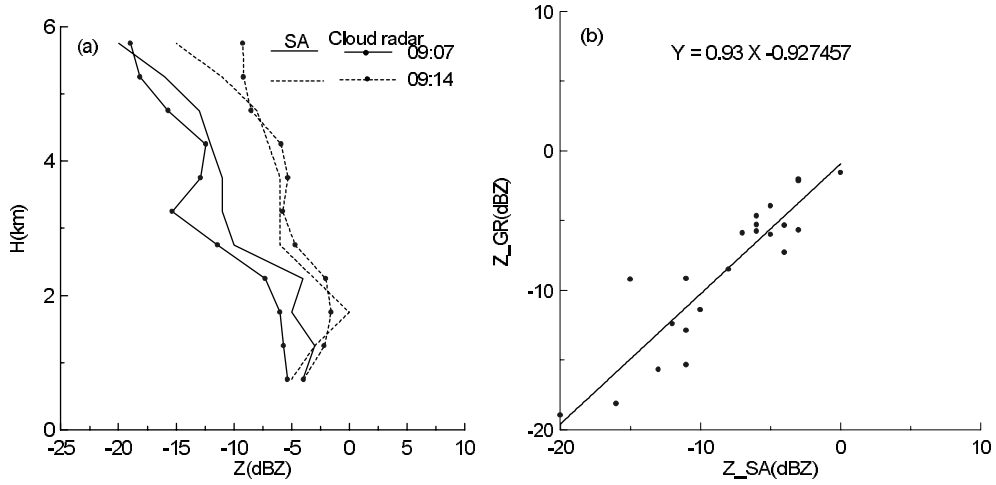

Fig. 8. Reflectivity profiles for the ground-based cloud radar and SA radar at 0907 LST and 0914 LST (a) and the scattergraph for reflectivity observed by both radars (b).

route and over the ground-based cloud radar by the SA radar are also shown in Figs. 9c and d. We can see that the variation patterns are similar for the two radars.

The ground-based cloud radar data were remapped onto a vertical resolution of 100 m, and the bias, correlation coefficient and standard deviation between the two kinds of cloud radars were calculated. Table 5 shows the statistical parameters between 1.5 and 7.0 km MSL for the two periods. Similar to the above results, the reflectivity observed by the airborne cloud radar is 13.7 dB stronger than that of the ground-based cloud radar. The correlation is very good. Figure 10 shows the relationships between the two kinds of reflectivity.

From Figs. 4, 5, 8 and 9, we can see that the vertical profiles show obvious variation with respect to altitude in terms of reflectivity differences. Factors that possibly produce the uncertainty include: the observation region being located at the edge of the precipitation system (Fig. 3); different wavelengths, spatial resolution and observation volume; observation time; and attenuation for cloud radar.

It should be noted that the above analysis does not consider the effect of attenuation on the reflectivity observation with the Ka-band radar. The attenuation of cloud and precipitation is discussed next. The iterative correction for attenuation (Hildebrand, 1978) was used to simulate the effect of attenuation on reflectivity. The attenuation coefficient is calculated from reflectivity by

$$K = aZ^b\,, \tag{6}$$

where K is the specific attenuation; Z is the unattenuated reflectivity and a and b are known parameters. To distinguish between the cloud and precipitation attenuation, the coefficients of a, b are set for cloud and precipitation (Wang et al., 2011): Liquid cloud, reflectivity: approximately -30 to -10 dBZ, a=1.108, b=0.49; weak precipitation, reflectivity: approximately -10 dBZ to 10 dBZ, $a = 0.0001$, $b = 0.928$.

We used the averaged reflectivity profile data to simulate the attenuation effects, under the assumption that the radar was correctly calibrated. The preliminary simulation results showed that attenuation reduces the observed reflectivity by the ground-based cloud radar above 3 dB at an altitude of 4 km. In this case, the reflectivity bias between the airborne and ground-based cloud radars is 10.7 dB.

5. Discussion and conclusions

To analyze the observation capability and test the design principle and working mode of a space-based cloud radar in China, a prototype was installed on an airplane and used for precipitation observations over Tianjin in conjunction with ground-based cloud radar

Table 5. Comparison of the bias, correlation coefficient and standard deviation for reflectivity between the ground-based cloud radar, airborne cloud radar and SA radar at altitudes between 1.5 and 7 km.

Time (LST)	Samples	Bias (Z1–Z3)	Correlation coefficient	Standard deviation
0906	54	14.3	0.86	2.9
0912	54	12.9	0.82	3.4
Total	108	13.7	0.84	3.2

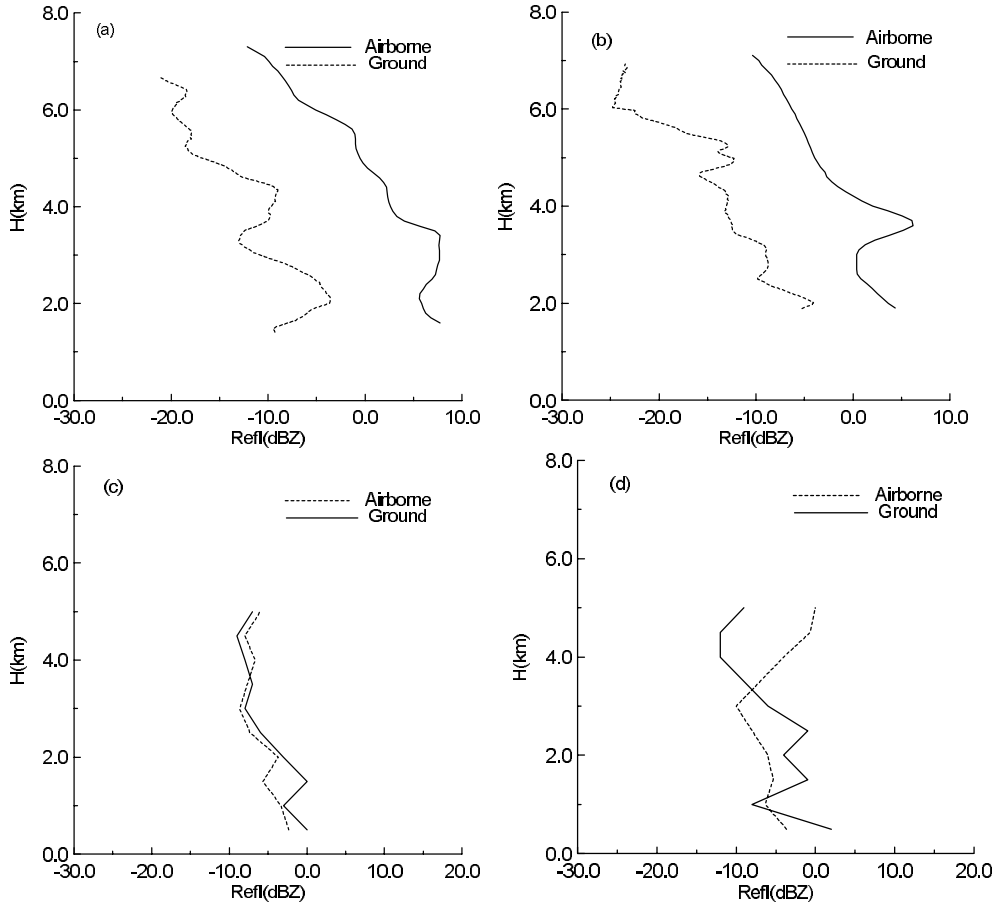

Fig. 9. Vertical profiles of reflectivity recorded by the airborne and corrected ground-based cloud radars: (a) averaged profiles between 0914 LST and 0921 LST recorded by the ground-based cloud radar (dotted line), as well as 0918 LST and 0921 LST recorded by the airborne radar (solid line); (b) the same as (a) but for 1015 LST and 1022 LST for the ground-based cloud radar, as well as 1021 LST and 1024 LST for the airborne radar; (c) averaged profiles of reflectivity recorded by the SA radar along the airplane's route (solid line) and over the ground-based radar (dotted line) during the first period; and (d) the same as (c), but for the second period.

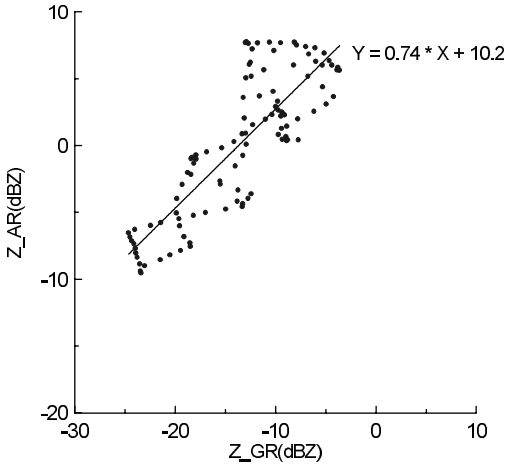

Fig. 10. Scattergram for 597 pairs of reflectivity by the SA radar and airborne cloud radar (AR).

and S-band operational radar. The ground-based S-band Doppler radar data and cloud radar data, collected on 10 July 2010, were analyzed to examine the observation capability of the prototype space-based cloud radar. The cross-comparison algorithm between different wavelengths, spatial resolutions and platforms radars has been presented. The vertical structures recorded by the three kinds of radars and the statistical parameters of observed reflectivity have been analyzed. The observational bias of reflectivity due to different wavelengths has been analyzed. The conclusions are as follows:

(1) The scattering properties of liquid particles with the S-band and Ka-band radar were calculated theoretically. The reflectivity bias due to wavelength was analyzed. The observation bias between Ka- and S-band radars for weak precipitation (Z<30 dBZ) was

negligible; for stronger precipitation, the bias was less than 5 dB.

(2) The three types of radar were able to resolve similar patterns of reflectivity profiles between altitudes of 1.5 and 4.0 km. The cloud radars were able to catch the detail of vertical variation. Ground clutter obscured the precipitation reflectivity below 1.5 km.

(3) Quantitative analysis on reflectivity bias between the different radars showed that the reflectivity with the airborne cloud radar was 10.9 dB stronger than with the SA radar, and 13.7 dB stronger than with the ground-based radar. The reflectivity recorded by the ground-based cloud radar was 0.4 dB weaker than that recorded by the SA radar. The probability distributions for reflectivity recorded by the SA and airborne cloud radars showed differences in weak and strong reflectivity regions. The attenuation of the Ka-band radar wavelength was able to increase the bias between the Ka- and S-band radars.

The results of this study should be repeated with more case studies, and the factors affecting the analysis of the results should be further considered. Importantly, the ground-based and airborne radars may not observe the same targets, the observation regions of the airborne and ground-based cloud radars were located at the edge of the precipitation system, and the spatial variation of reflectivity was not negligible. The difference between the two observed targets could have introduced uncertainty or errors in the analysis of results. Furthermore, the effects of attenuation on both of the cloud radars were different, which might also have caused errors in analysis. And lastly, the scattering volumes for the S-band and cloud radars were different. The SA radar performed volume scans with only nine elevation angles once every 5 min, thus producing a coarse vertical resolution of reflectivity and an uncertainty of bias between the SA and cloud radars.

The reasons for observational bias for the three kinds of radar could include the different work modes of the airborne and ground-based cloud radars, or the different calibration processes. The airborne and ground-based cloud radars worked in mechanical and phase array scanning modes, respectively. Research into, and the application of, cloud radar in China has only recently begun. In addition, a part of the phase array antenna of the space-based radar prototype was used in the airborne cloud radar, which could also have produced the observation error.

Acknowledgements. The authors wish to thank the Tianjin Meteorological Bureau for providing the SA radar data. This study was funded by the Chinese Academy of Meteorological Sciences Basic Scientific and Operational Project (observation and retrieval methods of microphysics and dynamic parameters of cloud and precipitation with multi-wavelength remote sensing), the National Key Program for Developing Basic Sciences under Grant 2012CB417202，the Meteorological Special Project (study and data process and key technology for space-borne precipitation radar) and the National Natural Science Foundation of China (Grant Nos. 40775021 and 41075098).

REFERENCES

Atlas, D., 1954: The estimation of cloud parameters by radar. *J. Meteor.*, **11**, 309–317.

Barber, P., and C. Yeh, 1975: Scattering of electromagnetic wave by arbitrarily shaped dielectric bodies. *Appl. Opt.*, **14** , 2864–2872.

Bolen, S. M., and V. Chandrasekar, 2000: Ground and satellite-based radar observation comparisons: Propagation of space-based radar signals. *IEEE International Geoscience and Remote Sensing Symposium*, **3**, 1352–1354.

Chandrasekar, V., V. N. Bringi, N. Balakrishnan and D. S. Zrnic', 1990: Error structure of multi-parameter radar and surface measurements of rainfall, Part III: Specific differential phase. *J. Atmos. Oceanic Technol.*, **7**, 621–629.

Danne, O., M. Quante, D. Milferstädt, H. Lemke, and E. Raschke, 1999: Relationships between Doppler spectral moments within large-scale cirro- and altostratus cloud fields observed by a ground-based 95-GHz cloud radar. *J. Appl. Meteor.*, **38**, 175–189.

Graeme, L. S., and Coauthors, 2002: The CLOUDSAT mission and the A-TRAIN. *Bull. Amer. Meteor. Soc.*, **83**, 1771–1790.

Hamazu, K., H. Hashiguchi, T. Wakayama, T. Matsuda, R. J. Doviak, and S. Fukao, 2003: A 35-GHz scanning Doppler radar for fog observations. *J. Atmos. Oceanic. Technol.*, **20**, 972–986.

Hildebrand, P. H., 1978: Iterative correction for attenuation of 5 cm radar in rain. *J. Appl. Meteor.*, **17**, 508–514.

Kollias, P., E. E. Clothiaus, M.A. Miller, E. P. Luke, K. L. Johnson, K. P. Moran, K. B. Widener, and B. A. Albrecht, 2007: The atmospheric radiation measurement program cloud profiling radars: Second-generation sampling stratrgies, processing and cloud data products. *J. Atmos. Oceanic Technol.,* **24**, 1119–1214.

Kropfli, R. A., and R. D. Kelly, 1996: Meteorological research applications of mm-wave radar. *Meteor. Atmos. Phys.*, **59**, 105–121.

Kropfli, R. A., B. W. Bartram, and S. Y. Matrosov, 1990: The upgraded WPL dual-polarization 8mm wavelength Doppler radar for microphysical and climate research. *Proc. Conf. on Cloud Physics*, Amer. Meteor. Soc., 492–494.

Lhermitte, R. M., 1987: A 94-GHz Doppler radar for cloud observations. *J. Atmos. Oceanic Technol.*, **4**,

36–48.

Marchand, R., G. G. Mace, T. Ackerman, and G. Stephens, 2008: Hydrometeor detection using Cloudsat—An earth-orbiting 94-GHz cloud radar. *J. Atmos. Oceanic Technol.*, **25**, 519–533.

Moran, K. P., B. E. Martner, M. J. Post, R. A. Kropfli, D. C. Welsh, and K. B. Widener, 1998: An unattended cloud-profiling radar for use in climate research. *Bull. Amer. Meteor. Soc.,* **79**, 443–455.

O'Connor, E. J., A. J. Illingworth, and R. J. Hogan, 2004: Retrieving stratocumulus drizzle parameters using Doppler radar and lidar. *J. Appl. Meteor.*, **44**, 14–27.

Paulsen, W. H., P. J. Petrocchi, and G. McLean, 1970: Operational utilization of the AN/TPQ-11 cloud detection radar. Air Force Cambridge Research Labs Instrumentation Papers, 166pp.

Pazmany, A. L., R. E. McIntosh, M. Hervig, R. Kelly, and G. Vali, 1994a: 95GHz polarimetric radar measurement of orographic cap clouds. *J. Atmos. Oceanic Technol.*, **11**, 140–153.

Pazmany, A. L., R. E. McIntosh, R. D. Kelly, and G. Vali, 1994b: An airborne 95 GHz polarized radar for cloud studies. *IEEE Trans. Geosci. Remote Sen.,* **32**, 731–739.

Plank, Vernon G., David Atlas, Wilbur H. Paulsen, 1955: The nature and detectability of clouds and precipitation as determined by 1.25-centimeter radar. *J. Meteor.*, **12**, 358–378.

Scarchilli, G., E. Gorgucci, V. Chandrasekar, and T. A. Seliga, 1993: Rainfall estimating using polarimetric technique at C-band frequencies. *J. Appl. Meteor.*, **32**, 1150–1160.

Sekelsky, S. M. and R. E. McIntosh , 1996: Cloud observation with a polarimetric 33 GHz and 95 GHz radar. *Meteor. Atmos. Phys.*, **59**, 123–140.

Ulbrich, C. W., 1983: Natural Variations in the analysis form of the raindrop size distribution. *J. Appl. Meteor.*, **22**, 1764–1775.

Vali, G., R. D. Kelly, A. Pazmany, and R. E. McIntosh, 1995: Airborne radar and in-situ observations of a shallow stratus with drizzle. *Atmospheric Research*, **38**, 361–380.

Wang, H. Y., L. P. Liu, G. L. Wang, W. Zhuang, J. Q. Zhang, and X. L. Chen. 2009: Development and application of the Doppler Weather Radar 3-D Digital Mosaic System. *Journal of Applied Meteorological Science*, **20**(2), 214–224. (in Chinese)

Wang, Z. H., X. Teng, L. Lei, and F. H. Zhao, 2011: A study of the relationship between attenuation coefficient and radar reflectivity factor for spherical particles in clouds at millimeter wavelengths. *Acta Meteorologica Sinica*, **69**(6), 1020–1028. (in Chinese)

Zhong, L. Z., L. P. Liu, S. Feng, R. S. Ge, and Z. Zhang, 2011: A 35-GHz polarimetric Doppler radar and its application in observing clouds associated with typhoon. *Adv. Atmos. Sci.*, **28**, 945–956, doi: 10.1007/s00376-010-0073-5.